

Characterization of the proteome and metabolome of human liver sinusoidal endothelial-like cells derived from induced pluripotent stem cells

Mathieu Danoy, Rachid Jellali, Yannick Tauran, Johanna Bruce, Marjorie Leduc, Françoise Gilard, Bertrand Gakière, Benedikt Scheidecker, Taketomo Kido, Atsushi Miyajima, et al.

▶ **To cite this version:**

Mathieu Danoy, Rachid Jellali, Yannick Tauran, Johanna Bruce, Marjorie Leduc, et al.. Characterization of the proteome and metabolome of human liver sinusoidal endothelial-like cells derived from induced pluripotent stem cells. Differentiation, 2021, 120, pp.1-26. 10.1016/j.diff.2021.06.001 . hal-03288696

HAL Id: hal-03288696
https://hal.utc.fr/hal-03288696

Submitted on 16 Jul 2021

HAL is a multi-disciplinary open access archive for the deposit and dissemination of scientific research documents, whether they are published or not. The documents may come from teaching and research institutions in France or abroad, or from public or private research centers.

L'archive ouverte pluridisciplinaire **HAL**, est destinée au dépôt et à la diffusion de documents scientifiques de niveau recherche, publiés ou non, émanant des établissements d'enseignement et de recherche français ou étrangers, des laboratoires publics ou privés.



Distributed under a Creative Commons Attribution 4.0 International License

Characterization of the proteome and metabolome of human liver sinusoidal endothelial-like cells derived from induced pluripotent stem cells.

Mathieu Danoy[1,2], Rachid Jellali[3], Yannick Tauran[4], Johanna Bruce[5], Marjorie Leduc[5], Francoise Gilard[6], Bertrand Gakière[6], Benedikt Scheidecker[1,2], Taketomo Kido[7], Atsushi Miyajima[7], Fabrice Soncin[1,8], Yasuyuki Sakai[2], Eric Leclerc[1,3*]

[1] CNRS UMI 2820; Laboratory for Integrated Micro Mechatronic Systems, Institute of Industrial Science, University of Tokyo; 4-6-1 Komaba; Meguro-ku; Tokyo, 153-8505, Japan

[2] Department of Chemical System Engineering, graduate school of Engineering, the University of Tokyo, 7-3-1, Hongo, Bunkyo-ku, Tokyo, 113-8656, Japan

[3] Université de technologie de Compiègne, CNRS, Biomechanics and Bioengineering, Centre de recherche Royallieu CS 60319, 60203, Compiègne Cedex, France

[4] Univ Lyon, Université Claude Bernard Lyon 1, Laboratoire des Multimatériaux et Interfaces, UMR CNRS 5615, F-69622 Villeurbanne, France

[5] Plateforme protéomique 3P5, Université de Paris, Institut Cochin, INSERM, CNRS, F-75014, France

[6] Plateforme Métabolisme Métabolome, Institute of Plant Sciences Paris-Saclay (IPS2), CNRS, INRA, Univ. Paris-Sud, Univ. Evry, Univ. Paris-Diderot, Univ. Paris Saclay, Bâtiment 630 Rue Noetzlin, 91192 Gif-sur-Yvette cedex, France

[7] Laboratory of Stem Cell Therapy, Institute for Quantitative Biosciences, The University of Tokyo, 1-1-1 Yayoi, Bunkyo-ku, Tokyo, 113-0032, Japan

[8] CNRS/IIS/Centre Oscar Lambret/Lille University SMMiL-E Project, CNRS Délégation Nord-Pas de Calais et Picardie, 2 rue de Canonniers, Lille, Cedex 59046, France

* corresponding author: Eric Leclerc

Abstract

The liver is a complex organ composed of several cell types organized hierarchically. Among these, liver sinusoidal endothelial cells (LSECs) are specialized vascular cells known to interact with hepatocytes and hepatic stellate cells (HSCs), and to be involved in the regulation of important hepatic processes in healthy and pathological situations. Protocols for the differentiation of LSECs from human induced pluripotent stem cells, hiPSCs, have been proposed and in-depth analysis by transcriptomic profiling of those cells has been performed. In the present work, an extended analysis of those cells in terms of proteome and metabolome has been implemented. The proteomic analysis confirmed the expression of important endothelial markers and pathways. Among them, the expression of patterns typical of LSECs such as *PECAM1, VWF, LYVE1, STAB1* (endothelial markers), *CDH13, CDH5, CLDN5, ICAM1, MCAM-CD146, ICAM2, ESAM* (endothelial cytoskeleton), *NOSTRIN, NOS3 (Nitric Oxide endothelial ROS), ESM1, ENG, MMRN2, THBS1, ANGPT2* (angiogenesis), *CD93, MRC1* (mannose receptor), *CLEC14A* (C-type lectin), CD40 (antigen), and *ERG (transcription factor)* was highlighted. Besides, the pathway analysis revealed the enrichment of the endocytosis, Toll-like receptor, Nod-like receptor, Wnt, Apelin, VEGF, cGMP-PCK, and PPAR related signaling pathways. Other important pathways such as vasopressin regulated water reabsorption, fluid shear stress, relaxin signaling, and renin secretion were also highlighted. At confluence, the metabolome profile appeared consistent with quiescent endothelial cell patterns. The integration of both proteome and metabolome datasets revealed a switch from fatty acid synthesis in undifferentiated hiPSCs to a fatty oxidation in LSECs and activation of the pentose phosphate pathway and polyamine metabolism in hiPSCs-derived LSECs. In conclusion, the comparison between the signature of LSECs differentiated following the protocol described in this work, and data found in the literature confirmed the particular relevance of these cells for future *in vitro* applications.

Keywords: Liver Sinusoidal Endothelial Cells, LSECs, human induced pluripotent stem cells, hiPSCs, proteomic, metabolomic

1. Introduction

Liver sinusoidal endothelial cells (LSECs) are the most abundant non-parenchymal cells in the liver, form a very specialized microvasculature, and play an important role in hepatic functions and diseases (De Smedt et al., 2021; Poisson et al., 2017). Those cells possess morphological features specific to the liver and differ from vascular endothelial cells by the lack of basal membrane and by the presence of large pores called fenestrae (Poisson et al., 2017). The fenestrae, clustered in sieve plates, allows bidirectional mass transfer between blood (mixture of arterial and venous content) and hepatocytes (transforming unit, Poisson et al., 2017; Gage et al., 2020). LSECs also exhibit high endocytotic activity for macromolecular waste products, due to the presence of a high density of endocytic vesicles (Braet and Wisse 2002, Poisson et al., 2017). Among other functions, LSECs contribute to the regulation of sinusoidal flow, to the maintenance of hepatic stellate cell quiescence, to liver regeneration, and are involved in hepatic complications such as fibrosis, cirrhosis, and hepatocellular carcinoma (Braet and Wisse 2002, Poisson et al., 2017).

The lack of complex *in vitro* models including mature and functional human Liver Sinusoidal Endothelial Cells (LSECS) remains one of the bottleneck problems for the pharmaceutical industry to provide relatively low-cost toxicological data and predictive information on the effects of xenobiotics in complex hepatic models. In that regard, promising alternatives such as the differentiation and maturation of human-induced pluripotent stem cells (hiPSCs) have been developed. As such, several investigations have led to the differentiation of hepatocyte-like cells (HLCs) from hiPSCs (Si Tayeb et al., 2010, Danoy et al., 2020, Kido et al., 2015). In parallel, hiPSCs have also been used to provide a reliable source for other hepatic cells such as HSCs (Coll et al., 2018) and LSECs (Koui et al., 2017). In this frame, hiPSCs have been differentiated toward an LSECs phenotype in which immunostaining coupled to Western blotting confirmed expression of important LSECs markers such as Stabilin-2 (Koui et al., 2017). Transcriptome analysis with the nano Cap Analysis Gene Expression (nanoCAGE) method was then performed to further confirm the overall vascular commitment of the cells (upregulation of the APLN, LYVE1, VWF, ESAM, and ANGPT2 genes). The analysis of promoter motif activities highlighted several transcription factors (TFs) of interest during the LSECs differentiation from iPSCs (IRF2, ERG, MEIS2, SPI1, IRF7, WRNIP1, HIC2, NFIX_NFIB, BATF, and PATZ1). Based on this investigation, a

regulatory network involving the relevant TFs, their target genes as well as their related signaling pathways was proposed (Danoy et al., 2020). In the present paper, to extend the characterization of the hiPSCs-derived LSECs produced by the differentiation protocol of Koui et al., 2017, their proteome and metabolome profiles were investigated. The panel of signatures and pathways highlighted by those analysis and their integration were then discussed with datasets from both *in vivo* and *in vitro* studies.

2. Material and methods

2.1. hiPSCs culture and differentiation protocol

The hiPSCs used in this study (454E2) were provided by the cell bank of the Riken BioResource Research Center (RIKEN BRC). 454E2 hiPSCs were cultured and differentiated following the protocol previously described by Koui et al., (2017). After differentiation, the cells were harvested and stored in liquid nitrogen. When required, the needed number of cells was seeded on plates (1.5 x 10^4 cells/cm^2) coated with fibronectin (20 µg/mL, Life Technologies) for 1 hour at 37°C, for further culture and proliferation for 9 days.

2.2. Metabolomic analysis

The global metabolomic profiling was performed with culture media (basal & used in culture, culture medium) using gas chromatography coupled to quadrupole mass spectrometry (GC-MS). Before the GC-MS analysis, an extraction step was performed on the culture media, according to the protocol previously described in (Jellali et al., 2018). Samples were analyzed by Agilent 7890B gas chromatograph coupled with an Agilent 5977A mass spectrometer. Separation was achieved on a Rxi-5SilMS column from Restek (30 m with a 10 m Integra-Guard column - ref 13623-127). The data files obtained were analyzed using the AMDIS software (http://chemdata.nist.gov/mass-spc/amdis/). Peak areas were determined using Masshunter Quantitative Analysis (Agilent) and normalized to ribitol. Metabolite contents are expressed in arbitrary units. The complete protocol is detailed in Supp File 1.

2.3. Proteomic analysis

The protocol for the preparation of proteins preparation protocol has been previously described (Danoy et al., 2020, details in Supp. File 1). Briefly, the protein samples were digested using trypsin, and the peptides were separated into 5 fractions. After speed-vacuum drying, fractions were solubilized in 10 µL of 0.1% TFA, 10% ACN. Liquid chromatography and mass spectrometry analyses were performed on an U3000 RSLC nanoflow-HPLC system coupled to an Orbitrap fusion MS analysis (Thermo Fisher Scientific). The Maxquant software was used to identify and quantify proteins. The database used was a concatenation of human sequences from the Uniprot-Swissprot database (Uniprot, release 2018-06) and an incremented list of contaminants. False discovery rate (FDR) was kept below 1% on both peptides and proteins.

2.4. Data statistical analysis

The multivariate statistical analysis of proteomic and metabolomic data were performed using XLSTAT software and MetaboAnalyst, a web-based platform for metabolomics data analysis (Chong et al., 2018). Supervised Partial Least Squares-Discriminant Analysis (PLS-DA) was carried out to discover significant variations between the groups. The quality of the PLS-DA model was evaluated by the R^2Y (fitting degree) and Q^2 (prediction parameter) values. The variable importance for the projection (VIP) parameter was used to select variables that had the most significant contribution in discriminating between both groups. VIP is a weighted sum of squares of the PLS weight that indicates the importance of each variable to the whole model. In parallel, univariate statistics were performed with Student's t-test, and *P-value* less than 0.05 was considered statistically significant. Variables with significant changes in the groups *(P-value* < 0.05 and VIP > 1) were selected as discriminating variables. Finally, MetaboAnalyst and Idep9.1/KEGG were used for pathway enrichment analysis of metabolomic and proteomic data, respectively.

3. Results

3.1. Cell morphology

After differentiation, LSECs were plated and amplified until they reached the confluence. The typical morphologies observed are presented in Fig. 1A-B. Notably, the cells displayed a comparable morphology to their primary counterpart, cultured in similar conditions (Fig. 1C). They formed a confluent, cobblestone-like, monolayer with large nuclei typical of endothelial morphology.

3.2. Characterization of the proteome profile of hiPSCs-derived LSECs

The proteome analysis of undifferentiated hiPSCs vs hiPSCs-derived LSECs was performed on 3187 positively identified proteins (Supp. File 2) to assess the changes in protein expression through the differentiation. The comparison led to the identification of 2537 proteins differentially expressed with a p_value below 0.05. The multivariate analysis allowed to separate hiPSCs-derived LSECs and hiPSCs as shown in Fig. 2A-B. The top 50 proteins differentially expressed in the PLS analysis are shown in the heatmap of Fig. 2C. Among the proteins overexpressed in hiPSCs, *FASN* (fatty acid synthetase), *HSP90AB1, FKBP4* (protein interaction at the estrogen receptor), *PSAT1, PHGDH* (Amino Acid metabolism), and *CEBPZ* were identified as discriminant proteins. hiPSCs-derived LSECs were characterized as expressing high levels of *CPT1A, HADHA* (involved in the fatty acid beta-oxidation), *OGDH* (TCA), *ITGB1, MYH9, ACTN4, FLNB, VIM, THBS1* (tight junction, focal adhesion, regulation of actin), *CD93* (receptor for mannose-binding leptin) which confirms the changes in metabolism occurring during the differentiation.

To verify that the differentiation engaged hiPSCs into a LSEC phenotype, the previously identified proteins were sorted by fold change. Within those proteins, the top-100 proteins over-expressed in hiPSCs-derived LSECs included several important endothelial markers such as *PECAM1, vWF, CDH13, THBS1, ICAM1, ANGPT2, CDH5, ESAM, CLDN5, ITGA5, ITGA3, ENG, ESM1, MCAM (CD146), CD93, MMRN2, CAV1, NOSTRIN, and ICAM2*. Specific LSECs markers such as *LYVE1*, *STAB1,* and *CD36* were also found in these top-100 proteins over-expressed in hiPSCs-derived LSECs. When the analysis was performed on the top-250 proteins over-expressed in hiPSCs-derived LSECs, ACE, NRP2, *PLVAP, ERG, MRC1* (a mannose receptor), *CLEC14A* (a C-type lectin), *and AQP1* were additionally identified. The complete signature extracted from this study is presented in Table 1.

To extract pathways specific to the hiPSCs-derived LSECs, proteins with a fold change above 1.2 / below 0.8 and with the *P-value* < 0.05 (579 proteins) and all proteins with *P-value* < 0.05 (2537 respectively) were input in the KEGG pathway database. The complete list of proteins used, and pathways extracted is given in Supp. File 2. Important LSECs and endothelial cells related pathways were expressed in hiPSCs-derived LSECs (Table 2). Among those were found C-type lectin receptor signal (4 and 15 hits respectively with the 579, and 2537 proteins lists), endocytosis (17 and 76 hits), NOD-like receptor signaling (12 and 33 hits), TOLL like receptor (2 and 12 hits), Apelin signaling (8 and 31 hits), VEGF signaling (2 and 11 hits), vascular smooth muscle contraction (5 and 24 hits), Wnt signaling (1 and 22 hits), cGMP-PCK signaling (7 and 24 hits), Vasopressin regulated water reabsorption (2 and 14 hits), PPAR signaling (7 and 21 hits), fluid shear stress (9 and 34 hits), relaxin signaling (8 and 25 hits), and renin secretion (6 and 11 hits). Targets in the HIF (5 and 28 hits) and FOXO (5 and 19 hits) signaling pathways were also found (gene names in pathways are given in Supp. File 2).

The extracted pathways were further arranged using iDEP.91. In that regard, a heatmap of the most discriminating biological processes extracted by the Gene Set Enrichment Analysis which characterized the profiles of hiPSCs and the hiPSCs-derived LSECs was created (Fig. 3A). The hierarchical clustering of the important biological processes enriched by the proteins, extracted by Desq2 analysis was also created (Fig. 3B, Supp. File 2 for the list of genes in each pathway). It was found that the profile of hiPSCs was characterized by biological processes such as RNA process, DNA process, and cell cycle while the hiPSCs-derived LSECs' profile was characterized by vesicle transport, sprouting angiogenesis, IL12 production, calcium-related signaling, and endo/exocytosis processes.

3.3. Characterization of the metabolome profile of hiPSCs-derived LSECs

Further characterization of hiPSCs-derived LSECs was done by screening for secreted metabolites. In that regard, the metabolomic analysis was performed and allowed to identify 86 metabolites (Supp. File 3). The multivariate analysis contributed to separate the basal medium and the used in culture with hiPSCs-derived LSECs, culture medium (Fig. 4A-B). The top 30 metabolites differentially present in both culture media included elements related to the consumption of amino acids (leucine, valine),

TCA substrates (citramalic acid, succinic acid, pyruvic acid), carbohydrate (mannitol, glucose), and lipid-related compounds (glyceric acid, azelaic acid). In parallel, the production of several amino acids (glycine, threonine, phenylalanine, proline, trans-4 hydroxy-proline), carbohydrates (mannose, fructose, tagatose, xylulose, lyxose, sorbitol, threitol, oxalic acid (TCA-derived metabolite), glycolic acid (TCA-derived metabolite, from xylulose metabolism), picolinic acid (metabolites of tryptophan metabolism), benzoic acid, ethanolamine, putrescine, and glycerol was also confirmed. Among those metabolites, 26 were found to be differentially present in both media with a P-value below 0.05 (Fig. 4C). Pathway analysis on those revealed phenomena such as enrichment of the galactose metabolism, glucose-alanine cycle, the fructose-mannose degradation, Warburg effect, gluconeogenesis. Various amino acid metabolisms, glycolysis, and pathways related to the metabolism of TCA were also highlighted (Fig. 5A-B, Supp File 3). Enrichment pathway analysis, using KEGG as a database, highlighted the valine-leucine isoleucine biosynthesis, Aminoacyl-tRNA biosynthesis, and Galactose metabolism as the top 3 pathways (Supp File 3).

4. Discussion

In the present study, the proteomic and metabolic profiles of hiPSCs-derived LSECs were extracted to evaluate the quality of the differentiated cellular model. Those results complete the histologic and transcriptomics analysis previously performed (Danoy *et al.*, 2020). In this previous study, hiPSCs-derived LSECs were shown to exhibit typical patterns of LSECs as compared to their primary counterpart. In addition, the cells were also found to be Stabilin-2$^+$, Stabilin-1$^+$, CD144$^+$, and CD31$^+$. In Table 2, the signature observed for the proteomic and metabolomic analysis of hiPSCs-derived LSECs was compared to other LSECs signatures found in the literature. In details, LSECs are typically characterized by a specific signature including markers such as *VEGFR3*$^+$, *VEGFR2*$^+$, *VE-Cadherin*$^+$, *FactorVIII*$^+$ *(VWF), CD34*$^-$, *CD45*$^-$ (Ding et al., 2010; Poisson et al., 2017) or *CD31*$^+$, *LYVE- 1*$^+$, *L-SIGN*$^+$, *Stabilin-1*$^+$, *CD34*$^-$, *PROX-1*$^-$ cells (Lalor et al., 2006, Poisson et al., 2017). In hiPSCs-derived LSECs, the proteome signature was characterized as *CD34*$^-$, *CD45*$^-$, *PROX1*$^-$, *CD31*$^+$, *LYVE1*$^+$, *STAB1*$^+$, *VE Cadherin*$^+$ *(CDH5), VWF*$^+$, *VEGFR2*$^+$, and completed by the expression of *CD146* (marker common in several types of endothelial cells), *CLEC14A* (C type

lectin), *CD93*, *MRC1* (both mannose receptors), and *NOS3* (nitric oxide endothelial ROS) as shown in Table 1. Notably, *and VEGFR3 and L-SIGN* were not detected in the proteome signature of hiPSCs-derived LSECs and major mature LSECs markers including *CD4* and *CD32*, and immature markers such as *CD34, 1F10* (Poisson et al., 2017), *CD4, CD32, CD34,* and *1F10* proteins were not expressed in this cellular model either.–Concerning CD31, it can be noted that this adhesion molecule, which is expressed in several endothelial cells, including in LSECs, is known to disappear in the latter with the establishment of fenestration (De Leve et a., 2004). Thus, the fact that hiPSCs-derived LSECs co-express *PECAM* and *ICAM1* illustrates that fenestration is probably not achieved in the current cellular model. This is in agreement with previously published results (Koui et al., 2017), and is also widely observed in models of LSECs cultured as a 2D monolayer (Lalor et al., 2006). Finally, a brief comparison between the proteomic signatures from the literature (HUVECs, as a positive control, and fibroblasts, as a negative control) was performed to further confirm the quality of the cellular model. In HUVECs, LSECs markers such as CD36, LYVE1, and STAB2 were not expressed while NRCAM, F11R, CEACAM21, CEACAM19, CADM4, CADM3, CADM1, JAM2, CDON, SELE were found to be expressed, but not in hiPSCs-derived LSECs (Madugundu et al., 2019).

The metabolic signature of LSECs is usually found to be highly variable depending on their state. In their quiescent state, endothelial cells are characterized by intense fatty acid oxidation and moderate glycolysis (Dumas et al., 2020). As migratory phenomena are induced, a switch to the production of lipids for membrane fluidity is usually observed (Dumas et al., 2020). As proliferation is induced, endothelial cells were characterized by intense glycolysis and glutamine breakdown, moderate fatty acid oxidation, oxidative phosphorylation, and serine biosynthesis (Dumas et al., 2020). In Table 3, the metabolomic profile observed in the presented analysis of hiPSCs-derived LSECs was synthesized and compared to the metabolomic profile of quiescent, migratory, and proliferative endothelial cells found in the literature. In the presented cellular model, the profile was found to be typical of beta-oxidation as shown by the low levels of azelaic acid. Besides, consumption of several TCA substrates, which reflects glycolytic activity was observed while no change in the levels of glutamine and serine was found. High levels of PPP intermediates such as sorbitol, xylulose could also be observed. As the analysis was performed on confluent hiPSCs-

derived LSECs, the profile observed would illustrate a quiescent-like phenotype rather than a proliferative behavior.

By integrating both the proteomic and metabolomic profiles of hiPSCs-derived LSECs, characterization of the cellular model was further performed. Pattern recognition receptors and components of inflammatory response usually expressed in LSECs include endocytosis receptors, Toll-like receptors, and Nod-like receptors (DeLeve et al., 2017). The enrichment of both Toll-like receptors and Nod-like receptors signaling (12 and 33 hits with P-value < 0.05 resp.) was confirmed in the present analysis. Regarding endocytosis, known to be one of the major functions of LSECs in the normal liver, it could be highlighted as illustrated by the KEGG endocytosis pathway (76 hits with P-value <0.05), and the C-type lectin receptor signaling (15 hits, P-value <0.05). Also, the LSECs endocytose is known to involve the scavenger receptor (SR), the mannose receptor, and the FC gamma receptor IIb2. Notably, the main known SRs are SR-H/Stabilin 1 and SR-H/Stabilin 2 (Poisson et al. 2017; DeLeve et al., 2017). The presence of STAB2 was also confirmed by western blot in the current cellular model (Danoy et al., 2020; Koui et al 2017) while mannose was detected in the metabolome as a significantly modulated molecule which further confirms the endocytosis function of the presented cellular model.

Endocytosis is also known to be involved in the regulation of the transport of lipids which is also one of the major functions of LSECs (Hammoutene et al., 2019). Furthermore, lipids have also been found to promote LSECs proliferation as well as the maintenance of their differentiation (Hang et al., 2012). The present dataset suggests a switch in the lipid metabolism in the differentiation of hiPSCs into LSECs. At the proteome level, this could be characterized by the overexpression of *FASN* in hiPSCS (fatty acid synthetase), and of *CPT1A* and *HADHA* (fatty acid beta-oxidation) in hiPSCs-derived LSECs which implies a degradation of fatty acid as this would be the case in mature LSECs. Besides, lipid homeostasis was highlighted via PPAR signaling in the proteome dataset while the fatty acid degradation was illustrated by the consumption of azaelic acid in the metabolome dataset. hiPSCs-derived LSECs also exhibited an activation of the pentose phosphate pathway (PPP) via the measured concentrations of xylulose and sorbitol which is consistent with the phenotype observed in healthy endothelial cells' phenotype (Dumas et al., 2020). Activation of the

PPP could further be confirmed via its function toward nucleotide synthesis for angiogenic activity (18 hits and 15 hits in nucleotide sugar metabolism and nucleotide excision repair respectively at the proteome level and production of putrescine, a substrate of polyamine at the metabolome level), antioxidant defense (overexpression of *GPX1, GPX2, GSTO1, MGST2, MGST3, GSTK1, GSTM3* in the proteome dataset), and nitric oxide synthesis (overexpression of *NOS3* in the proteome dataset) (Bierhansl et al., 2017) which further confirms the viability of the presented cellular model.

Nonetheless, this model still presents important limitations toward the complete reproduction of the *in vivo* phenotype of LSECs. Indeed, fenestration could not be observed in hiPSCs-derived LSECs (Koui et al., 2017) which is a strong impairment toward the function of the cells in fluid exchange and transport of molecules. Fenestration is known to be nitric oxide-dependent via the endogenous nitric oxide synthase (eNOS)-soluble guanylate cyclase (sGC)-cGMP pathway (DeLeve et al., 2017) for which the overexpression was found in the proteome dataset. However, one of the main sources of NO in the normal liver is known to be mediated via endothelial nitric oxide synthase (eNOS) activation by shear stress (Shah et al., 1997, Poisson et al., 2017), which is not reproduced in the current experimental setup. Subjection to shear stress is known to induce the KLF2 transcription factor (Gracia-Sancho et al., 2019, Poisson et al., 2017) which stimulates the endothelial upregulation of vasodilating agents such as nitric oxide (NO) (Poisson et al., 2017, Parmar et al., 2006). Although partial activation of shear stress-related markers (in the KEGG pathway) and vasoconstriction/vasodilation markers (via *THSB1*) could be confirmed, the lack of direct exposition to shear stress remains a major weakness in the current approach. Finally, further confirmation of the differentiation protocol is required with different hiPSCs lines, as biological variability has been observed (Volpato et al., 2020; Ortmann et al., 2020).

Conclusions

In this study, the analysis of the proteome and metabolome dataset of hiPSCs-derived LSECs was presented to assess the quality of this differentiated cellular model. The cell signature could be confirmed as characteristic of LSECs, expressing typical

vascular and endothelial markers in addition to LSEC specific proteins while important liver and LSEC patterns were also observed. Specifically, vital functions such as lipid metabolism, the pentose phosphate pathway, and the production of polyamine could be confirmed. In terms of future perspectives, the study of the hiPSCs-derived LSECs in conditions reproducing their *in vivo* microenvironment could help to further characterize the cells via exposition to shear stress and to other liver cell types in coculture.

Acknowledgments

This project was supported by the iLite ANR-16-RHUS-0005 and by a LIMMS internal funding. We acknowledge the 3P5 proteomic platform (Université de Paris, Institut Cochin, INSERM, U1016, CNRS, UMR8104, F-75014 PARIS, France*)* and François Guillonneau for their precious advice on the proteomic analysis and Cédric Broussard for monitoring the project. The Orbitrap Fusion mass spectrometer was acquired with funds from the FEDER through the « Operational Programme for Competitiveness Factors and employment 2007-2013 », and from the « Canceropole Ile de France. F.S. is an INSERM director of research. The authors also thank the JSPS Core-to-Core Program.

Authors contribution

M.D. designed, performed the experiments & the analysis, and participated in the writing of the manuscript. R. J. performed the analysis of the metabolome, the integration of the omics dataset, and participated in the writing of the manuscript. Y.T. designed & performed the protein extraction. J.B, M.L., and M.L.G. performed the analysis of the proteome. F.G. and B.G. performed the analysis of the metabolome. B.S. participated in the hiPSCs differentiation and human LSECs primary cultures. T.K. and A.M. participated in the design of the experiment and developed the LSECs differentiation protocol. F.S. participated in the data analysis and the writing of the

manuscript. Y. S. participated in the design of the experiment. E. L. participated in the design of the experiment, its analysis, and the writing of the manuscript.

Conflict of interest statement

The authors declare no conflict of interest.

Ethical issue

No ethical approval was required for the work presented in this study.

Figures captions

Figure 1: Morphology of hiPSCs-derived LSECs on Day 1 (A) and upon reaching confluence on Day 7 (B). Morphology of primary human LSECs upon reaching confluence on Day 5 (C).

Figure 2: Multivariate statistical analysis on proteomic profiles. PLS-DA scores plot discriminating hiPSCs-derived LSECs and hiPSCs (A). Volcano plot (log2 fold change (hiPSCs-derived LSECs/hiPSCs) plotted against −log10 P-value) highlighting proteins differentially expressed in hiPSCs-derived LSECs and hiPSCs ($P < 0.05$). Proteins upregulated and downregulated in hiPSCs-derived LSECs (compared to hiPSCs) are labeled in red and blue respectively (B). Heatmap of top 50 proteins differentially expressed in both conditions (C).

Figure 3: Important biological processes extracted with iDEP.91 in the comparison between hiPSCs-derived LSECs and hiPSCs proteome profile. Corresponding heatmap of the parametric gene set enrichment analysis in which red denotes

upregulated pathways; blue denotes downregulated pathways (A) and hierarchical clustering (B).

Figure 4: Multivariate statistical analysis of metabolomic profile. PLS-DA scores plot discriminating medium in culture with hiPSCs-derived LSECs and basal medium (A). Volcano plot (log2 fold change (medium in culture with hiPSCs-derived LSECs/basal medium) plotted against −log10 P-value) highlighting metabolites differentially expressed in culture with hiPSCs-derived LSECs and basal medium ($P < 0.05$). Metabolites upregulated and downregulated in the medium in culture with hiPSCs-derived LSECs (compared to basal medium) are labeled in red and blue respectively (1: citramalic ac, 2: pyruvic ac, 3: azelaic ac, 4: lactic ac, 5: ethanolamine, 6: xylulose, 7: mannose, 8: lyxose) (B). Heatmap of metabolites differentially expressed in both conditions (C).

Figure 5: Metabolic pathways analysis based on the metabolomic profile (in the comparison between medium in culture with hiPSCs-derived LSECs and basal medium). Pathway impact enrichment extracted from the analysis. 1: valine-leucine biosynthesis, 2: aminoacyl-tRNA biosynthesis, 3: galactose metabolism, 4: arginine and proline metabolism, 5: pyruvate metabolism, 6: phenylalanine, tyrosine, and tryptophan Biosynthesis, 7: TCA cycle (A). Top 20 pathways extracted by the metabolite set enrichment analysis (B).

Table 1: Signature of proteins overexpressed in hiPSCs-derived LSECs in the comparison with hiPSCs. Comparison with data found in the literature.

Table 2: Selected pathways related to the function of LSECs, and associated protein extracted with a p_value below 0,05 in the present analysis.

Table 3: Comparison of the metabolic profile of the hiPSCs-derived LSECs analyzed in the present analysis with profiles defined in the literature. Data reproduced from the review of Dumas et al., 2020.

References

Anil K. Madugundu, Chan Hyun Na, Raja Sekhar Nirujogi, Santosh Renuse, Kwang Pyo Kim, Kathleen H. Burns, Christopher Wilks, Ben Langmead, Shannon E. Ellis, Leonardo Collado-Torres, Marc K. Halushka, Min-Sik Kim, and Akhilesh Pandey, Integrated Transcriptomic and Proteomic Analysis of Primary Human Umbilical Vein Endothelial Cells, Proteomics. 2019 Aug; 19(15): 1800315.

Bierhansl, L., Conradi, L. C., Treps, L., Dewerchin, M., & Carmeliet, P. (2017). Central role of metabolism in endothelial cell function and vascular disease. *Physiology*, *32*(2), 126-140.

Chong, J., Soufan, O., Li, C., Caraus, I., Li, S., Bourque, G., ... & Xia, J. (2018). MetaboAnalyst 4.0: towards more transparent and integrative metabolomics analysis. *Nucleic acids research*, *46*(W1), W486-W494.

Coll, M., Perea, L., Boon, R., Leite, S. B., Vallverdu, J., Mannaerts, I., ... & Sancho-Bru, P. (2018). Generation of hepatic stellate cells from human pluripotent stem cells enables in vitro modeling of liver fibrosis. *Cell stem cell*, *23*(1), 101-113.

Danoy, M., Poulain, S., Koui, Y., Tauran, Y., Scheidecker, B., Kido, T., ... & Leclerc, E. (2020). Transcriptome profiling of hiPSC-derived LSECs with nanoCAGE. *Molecular omics*, *16*(2), 138-146.

DeLeve, L. D., Wang, X., Hu, L., McCuskey, M. K., & McCuskey, R. S. (2004). Rat liver sinusoidal endothelial cell phenotype is maintained by paracrine and autocrine regulation. *American Journal of Physiology-Gastrointestinal and Liver Physiology*, *287*(4), G757-G763.

DeLeve, L. D., & Maretti-Mira, A. C. (2017, November). Liver sinusoidal endothelial cell: an update. In *Seminars in liver disease* (Vol. 37, No. 4, p. 377). NIH Public Access.

Ding, B. S., Nolan, D. J., Butler, J. M., James, D., Babazadeh, A. O., Rosenwaks, Z., ... & Rafii, S. (2010). Inductive angiocrine signals from sinusoidal endothelium are required for liver regeneration. *Nature*, *468*(7321), 310-315.

Dumas, S. J., García-Caballero, M., & Carmeliet, P. (2020). Metabolic signatures of distinct endothelial phenotypes. *Trends in Endocrinology & Metabolism*.

Gracia-Sancho, J., Russo, L., García-Calderó, H., García-Pagán, J. C., García-Cardeña, G., & Bosch, J. (2011). Endothelial expression of transcription factor Kruppel-like factor 2 and its vasoprotective target genes in the normal and cirrhotic rat liver. *Gut*, *60*(4), 517-524.

Hammoutene, A., & Rautou, P. E. (2019). Role of liver sinusoidal endothelial cells in non-alcoholic fatty liver disease. *Journal of hepatology*, *70*(6), 1278-1291.

Hang, T. C., Lauffenburger, D. A., Griffith, L. G., & Stolz, D. B. (2012). Lipids promote survival, proliferation, and maintenance of differentiation of rat liver sinusoidal endothelial cells in vitro. *American Journal of Physiology-Gastrointestinal and Liver Physiology*, *302*(3), G375-G388.

Jellali, R., Gilard, F., Pandolfi, V., Legendre, A., Fleury, M. J., Paullier, P., ... & Leclerc, E. (2018). Metabolomics-on-a-chip approach to study hepatotoxicity of DDT, permethrin and their mixtures. *Journal of Applied Toxicology*, *38*(8), 1121-1134.

Kido, T., Koui, Y., Suzuki, K., Kobayashi, A., Miura, Y., Chern, E. Y., ... & Miyajima, A. (2015). CPM is a useful cell surface marker to isolate expandable bi-potential liver progenitor cells derived from human iPS cells. *Stem Cell Reports*, *5*(4), 508-515.

Koui, Y., Kido, T., Ito, T., Oyama, H., Chen, S. W., Katou, Y., ... & Miyajima, A. (2017). An in vitro human liver model by iPSC-derived parenchymal and non-parenchymal cells. *Stem cell reports*, *9*(2), 490-498.

Lalor, P. F., Lai, W. K., Curbishley, S. M., Shetty, S., & Adams, D. H. (2006). Human hepatic sinusoidal endothelial cells can be distinguished by expression of phenotypic

markers related to their specialised functions in vivo. *World journal of gastroenterology: WJG*, *12*(34), 5429.

Madugundu, A. K., Na, C. H., Nirujogi, R. S., Renuse, S., Kim, K. P., Burns, K. H., ... & Pandey, A. (2019). Integrated transcriptomic and proteomic analysis of primary human umbilical vein endothelial cells. *Proteomics*, *19*(15), 1800315.

Parmar, K. M., Larman, H. B., Dai, G., Zhang, Y., Wang, E. T., Moorthy, S. N., ... & García-Cardeña, G. (2006). Integration of flow-dependent endothelial phenotypes by Kruppel-like factor 2. *The Journal of clinical investigation*, *116*(1), 49-58.

Poisson, J., Lemoinne, S., Boulanger, C., Durand, F., Moreau, R., Valla, D., & Rautou, P. E. (2017). Liver sinusoidal endothelial cells: Physiology and role in liver diseases. *Journal of hepatology*, *66*(1), 212-227.

Sebastião, M. J., Pereira, R., Serra, M., Gomes-Alves, P., & Alves, P. M. (2018). Unveiling human cardiac fibroblast membrane proteome. *Proteomics*, *18*(13), 1700446.

Shah, V., Haddad, F. G., Garcia-Cardena, G., Frangos, J. A., Mennone, A., Groszmann, R. J., & Sessa, W. C. (1997). Liver sinusoidal endothelial cells are responsible for nitric oxide modulation of resistance in the hepatic sinusoids. *The Journal of clinical investigation*, *100*(11), 2923-2930.

Si-Tayeb, K., Noto, F. K., Nagaoka, M., Li, J., Battle, M. A., Duris, C., ... & Duncan, S. A. (2010). Highly efficient generation of human hepatocyte–like cells from induced pluripotent stem cells. *Hepatology*, *51*(1), 297-305.

Table 1: Signature of proteins overexpressed in hiPSCs-derived LSECs in the comparison with hiPSCs. Comparison with data found in the literature.

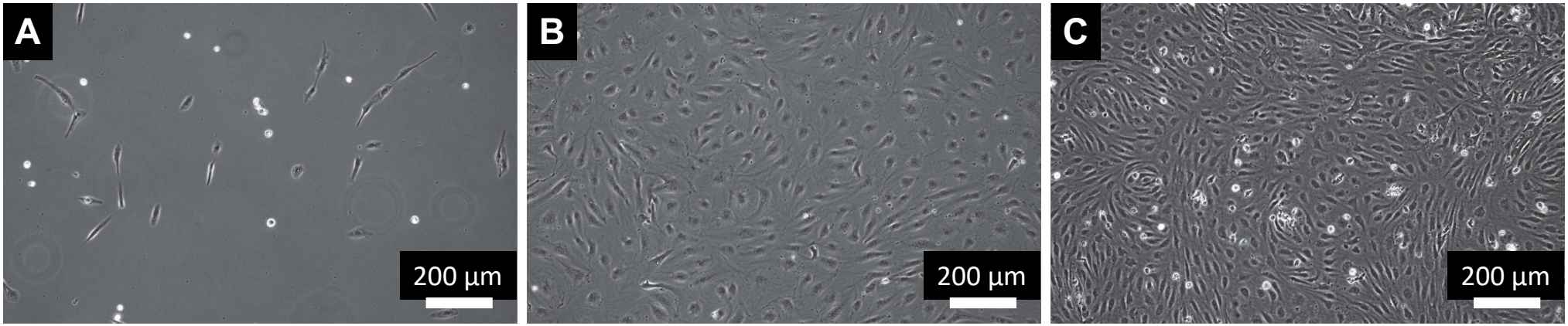
Proteomic signature oh hiPSCs-derived LSECs extracted from the present analysis			**Data from the literature**
Endothelial Markers	**FC (LSECs/hiPSCs)**	**Raw.pval**	**LSECs Markers**
PECAM1 (CD31)	1,8946	4,95E-05	Lalor et al., 2006; Poisson et al., 2017 *CD31^{+}, LYVE- 1^{+}, L-SIGN^{+}, Stabilin-1^{+}, CD34^{-} , PROX-1^{-}* Ding et al., 2010; Poisson et al 2017 *VEGFR3^{+}, VEGFR2^{+}, VE-Cadherin^{+}, FactorVIII^{+} (VWF), CD34^{-}, CD45^{-}*
vWF	1,7691	6,62E-08	
CDH13	1,5819	8,76E-08	
MMRN2	1,555	7,77E-07	
MCAM (CD146)	1,538	9,02E-05	
THBS1	1,5274	1,42E-08	
CD93	1,5114	1,42E-08	
ICAM1	1,4641	7,89E-07	
ANGPT2	1,4566	7,89E-06	
CDH5	1,4537	2,88E-05	
CAV1	1,451	1,63E-06	
ESAM	1,4421	4,73E-07	
CLDN5	1,4226	3,03E-05	
ITGA5	1,3886	2,59E-06	
ITGA3	1,3859	1,23E-05	
ENG	1,3813	9,11E-06	
NOSTRIN	1,3795	3,25E-05	
ESM1	1,3701	3,91E-05	
ICAM2	1,3661	0,0011909	
ACE	1,3586	1,71E-05	
NRP2	1,3533	2,24E-06	
PLVAP	1,3523	0,00013547	
ERG	1,2822	0,00084371	
LSECs Specific Markers	**FC (LSEC/hiPSCs)**	**raw.pval**	
LYVE1	1,6043	1,23E-06	
STAB1	1,5184	3,86E-07	
CD36	1,4815	2,94E-05	
MRC1	1,3299	0,00058979	
CLEC14A	1,3136	1,06E-05	
AQP1	1,2736	0,00010051	

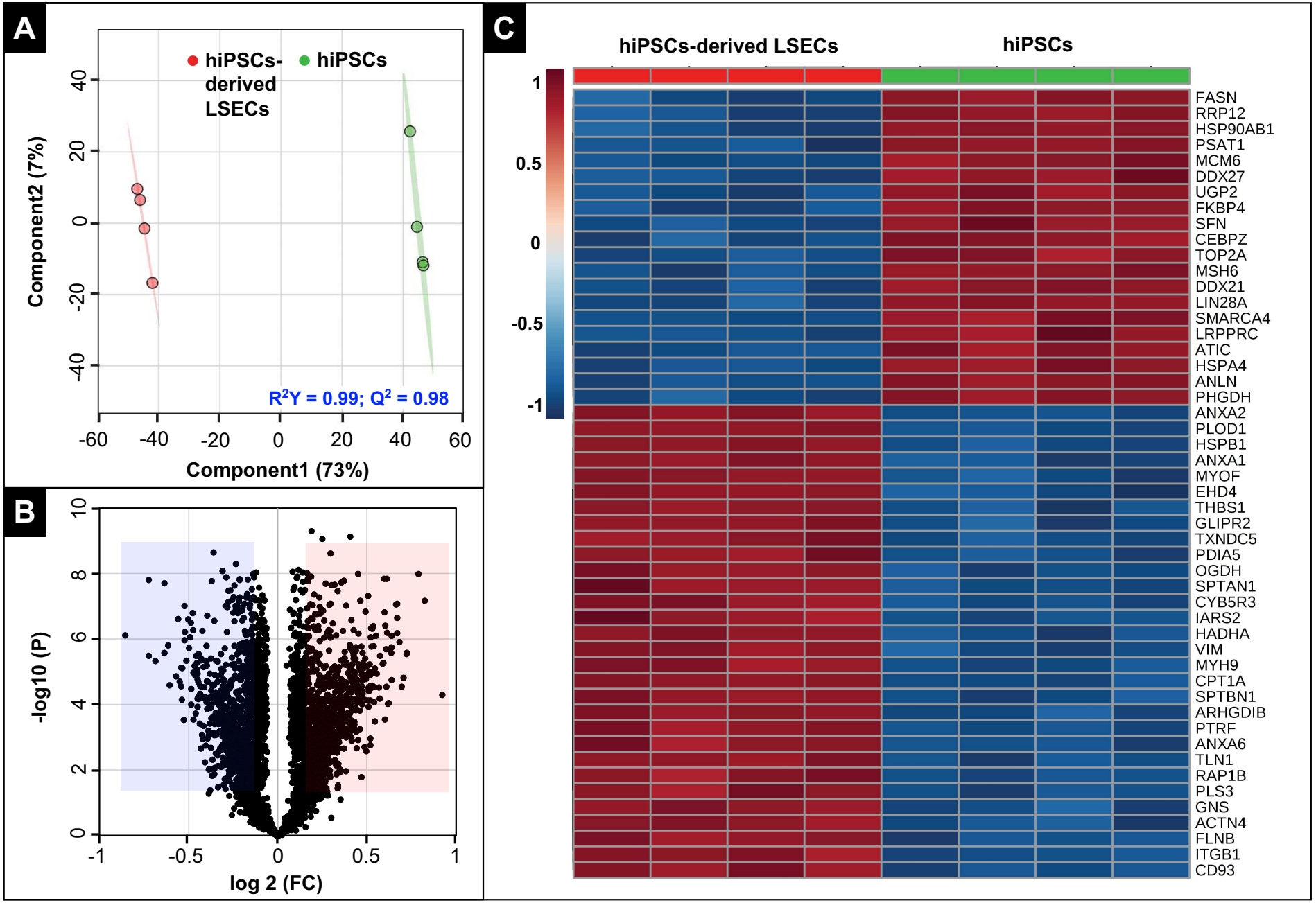
Table 2: Selected pathways related to the function of LSECs, and associated protein extracted with a p_value below 0,05 in the present analysis.

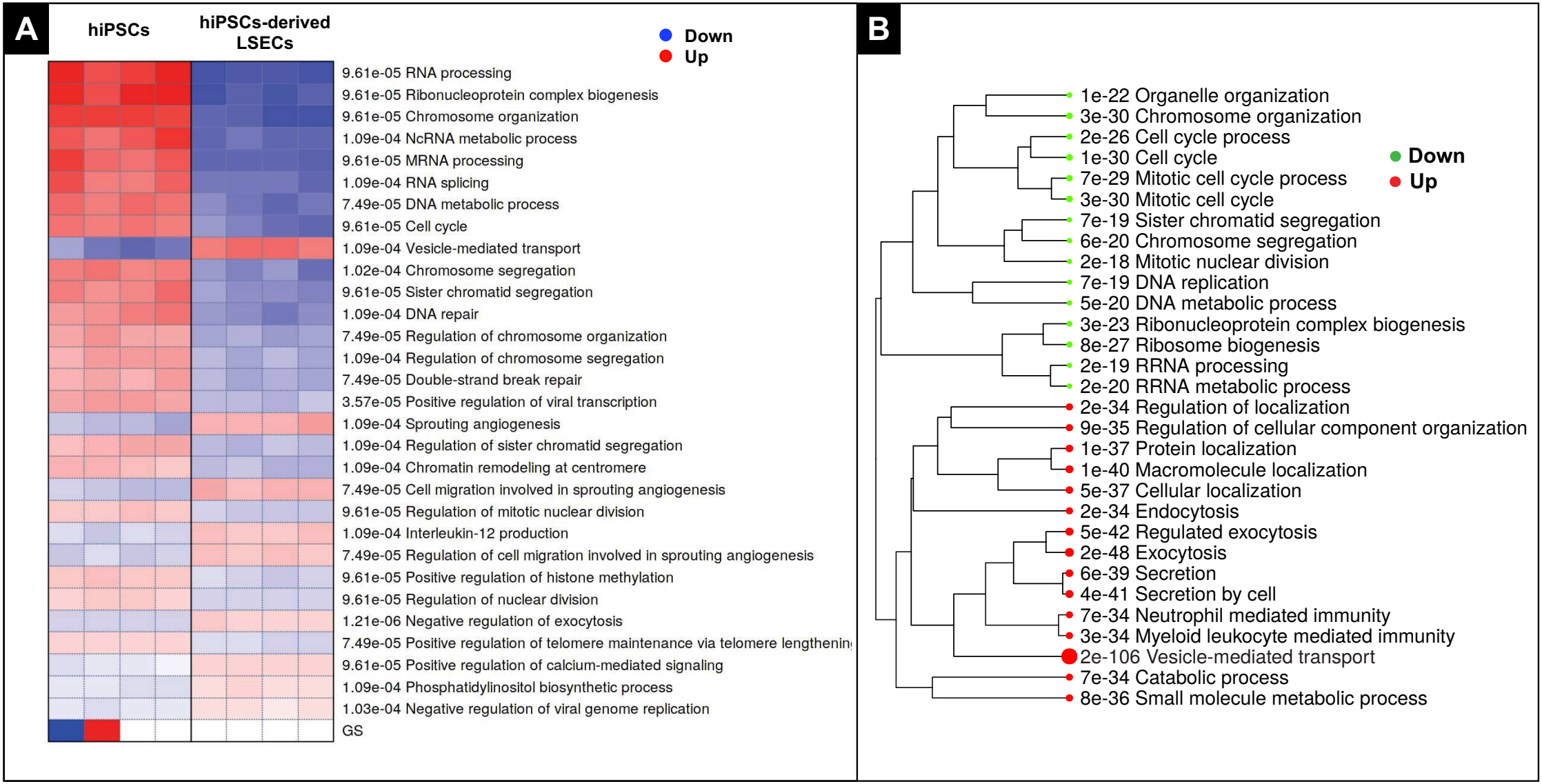
Pathway	Proteins
Endocytosis	ACAP2, AGAP3, AP2A2,AP2M1,ARAP1, ARAP3, ARFGAP3, ARFGEF1, ARPC1B, ARPC2, ARPC3, ARPC4, ARPC5, ARRB1, ARRB2, ASAP2, BIN1, CAPZA2, CAPZB, CAV1, CAV2, CDC42, CHMP3, DAB2, EEA1, EHD1,2,3,4, EPN2, GIT1,GIT2, HLA-A,-B-C, HSPA2, HSPA8, IQSEC1, IQSEC2, KIF5B, KIF5C, LDLRAP1, MVB12A, NEDD4, PARD3, PLD1, PML, PRKCI, RAB11FIP1, RAB11FIP5, RAB22A, RAB4AA, RAB5B, RAB5C, RAB7A, RABEP1, RHOA, RUFY1, SH3GLB1, SH3KBP1, SMAD3, SNX2,3,4,6, SPG21, SRC, TFRC, TGFBR2, VPS26A, VPS29, 35,36, 45, 4B, ZFYVE16
C-type lectin receptor	AKT1, CASP1,8, ITPR2,3, MAPK1,3, NFKB2, PAK1, PLCG2, RELA, RHOA, RRAS, RRAS2, SRC
Nod like receptor	CASP1,4,8, CTSB, GBP1,2, GSDMD, HSP90A1,B1, IFI16, IRAK4, IRF3, ITPR2,3, JAK1, MAP3K7, MAPK1, MAPK3, MAVS, NEK7, OAS2,3,PANX1,PKN1,2,PLCB1,2, RELA, RHOA, TANK, TBK1, TXNIP, XIAP
Toll like receptor	AKT1, CAPS8, CD40, IRAK4, IRF3, MAP3K7, MAPK1,3, RAC1, RELA, TBK1, TOLLIP
Wnt Signaling	CACYBP, CAMK2D, CAMk2G, CHD8, CTBP2, DVL2, EP300, GPC4, MAP3K7, PLCB1, PRKACA, PRKACB, PRKCA, RAC1, RHOA, ROCK2, RUVBL1, SFRP2, SKP1, SMAD3, TBL1XR1
VEGF signaling	AKT1, CDC42, HSPB1, KDR, MAPK1, MAPK3, NOS3, PLCG2, PRKCA, RAC1, SRC
cGMP-PKG signaling	AKT, ATP2B1, ATP2B4, GNA11,13,I2, GTF2I, ITPR2,3, MAPK1,3,MYL9, MYLK, NOS3, NPR1, PDE2A, PDE5A, PLCB1,2,PPIF, PPP1CC, RHOA, ROCK2, SLC25A5
Apelin signaling	AKT1, CDH1, GNA13, GNAI2, GNB1,2,4, GNG11,12, HDAC4, ITPR2, 3, JAG1, MAPK1,3 MTOR, MYLK, NOS3, PLCB1,2, PRKAA1, PRKAB1, PRKACA, PRKACB, RPS6, RRAS, RRAS2, SERPINE1, SLC9A1, SMAD3, TFAM
PPAR signaling	ACAA1, ACOX3, APOA1, CD36, CPT1A, CPT2, CYP27A1, EHHADH, FABP4, FABP5, FADS2, ILK, LPL, ME3, MMP1, PCK2, PLTP, SCD, SCP2, SLC27A1
Vasopressin regulated water reabsorption	ARHGDIA, ARHGDIB, DCTN1, DCTN2, DCTN4, DYNC2H1, DYNC1LI2, NSF, PRKACA, PRKACB, RAB5B, RAB5C, STX4, VAMP2

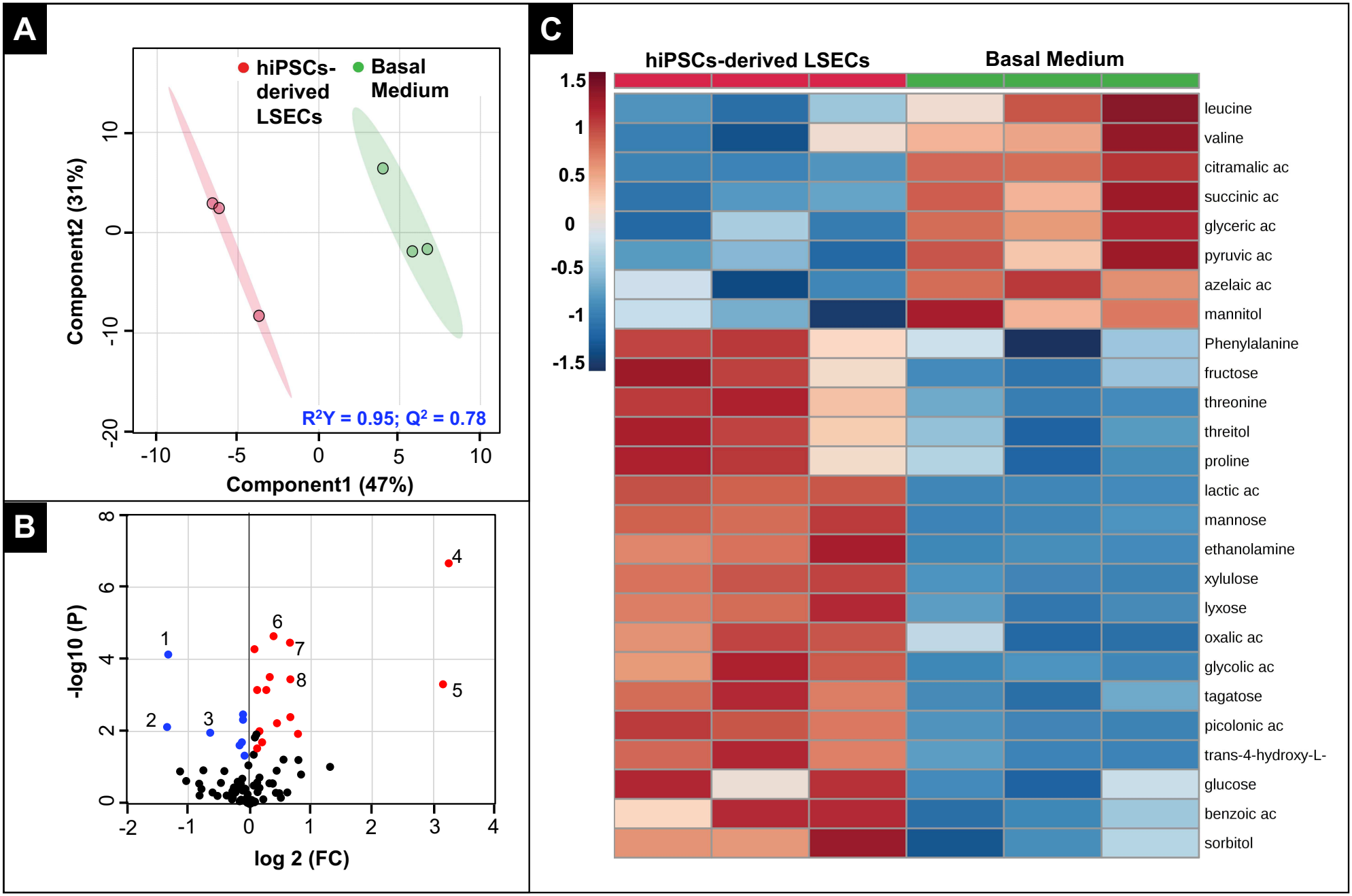
Table 3: Comparison of the metabolic profile of the hiPSCs-derived LSECs analyzed in the present analysis with profiles defined in the literature. Data reproduced from the review of Dumas et al., 2020.

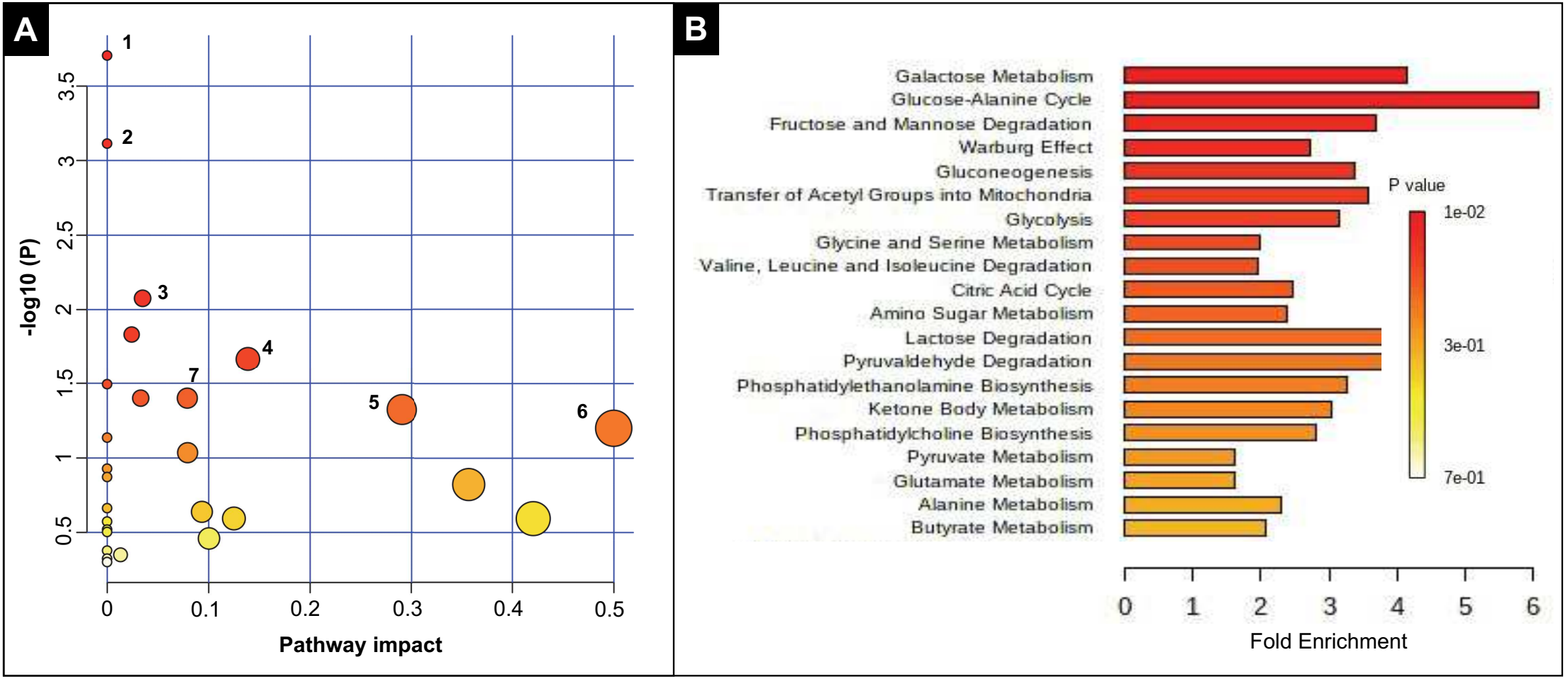
Profile extracted from the present analysis	**Quiescent Endothelial Cells**	**Migrating Endothelial Cells**	**Proliferative Endothelial Cells**
Low azelaic acid High glucose, fructose Low pyruvic acid Low succinic, citramalic acids (TCA) High sorbitol, xylulose No glutamine variation	High Fatty acid oxidation Moderate Glycolysis Oxidative pentose phosphate pathway	High Fatty acid synthesis High Glycolysis High Glutamine breakdown Proline biosynthesis Cholesterol transport	Moderate Fatty acid oxidation Fatty acid synthesis High Glycolysis High Glutamine breakdown Serine biosynthesis High OXPHOS respiration


A
200 µm
B
200 µm
C
200 µm


A
hiPSCs-derived LSECs
hiPSCs
Component2 (7%)
Component1 (73%)
R²Y = 0.99; Q² = 0.98
B
-log10 (P)
log 2 (FC)
C
hiPSCs-derived LSECs
hiPSCs
FASN
RRP12
HSP90AB1
PSAT1
MCM6
DDX27
UGP2
FKBP4
SFN
CEBPZ
TOP2A
MSH6
DDX21
LIN28A
SMARCA4
LRPPRC
ATIC
HSPA4
ANLN
PHGDH
ANXA2
PLOD1
HSPB1
ANXA1
MYOF
EHD4
THBS1
GLIPR2
TXNDC5
PDIA5
OGDH
SPTAN1
CYB5R3
IARS2
HADHA
VIM
MYH9
CPT1A
SPTBN1
ARHGDIB
PTRF
ANXA6
TLN1
RAP1B
PLS3
GNS
ACTN4
FLNB
ITGB1
CD93


A
hiPSCs
hiPSCs-derived LSECs
Down
Up
9.61e-05 RNA processing
9.61e-05 Ribonucleoprotein complex biogenesis
9.61e-05 Chromosome organization
1.09e-04 NcRNA metabolic process
9.61e-05 MRNA processing
1.09e-04 RNA splicing
7.49e-05 DNA metabolic process
9.61e-05 Cell cycle
1.09e-04 Vesicle-mediated transport
1.02e-04 Chromosome segregation
9.61e-05 Sister chromatid segregation
1.09e-04 DNA repair
7.49e-05 Regulation of chromosome organization
1.09e-04 Regulation of chromosome segregation
7.49e-05 Double-strand break repair
3.57e-05 Positive regulation of viral transcription
1.09e-04 Sprouting angiogenesis
1.09e-04 Regulation of sister chromatid segregation
1.09e-04 Chromatin remodeling at centromere
7.49e-05 Cell migration involved in sprouting angiogenesis
9.61e-05 Regulation of mitotic nuclear division
1.09e-04 Interleukin-12 production
7.49e-05 Regulation of cell migration involved in sprouting angiogenesis
9.61e-05 Positive regulation of histone methylation
9.61e-05 Regulation of nuclear division
1.21e-06 Negative regulation of exocytosis
7.49e-05 Positive regulation of telomere maintenance via telomere lengthenin
9.61e-05 Positive regulation of calcium-mediated signaling
1.09e-04 Phosphatidylinositol biosynthetic process
1.03e-04 Negative regulation of viral genome replication
GS
B
Down
Up
1e-22 Organelle organization
3e-30 Chromosome organization
2e-26 Cell cycle process
1e-30 Cell cycle
7e-29 Mitotic cell cycle process
3e-30 Mitotic cell cycle
7e-19 Sister chromatid segregation
6e-20 Chromosome segregation
2e-18 Mitotic nuclear division
7e-19 DNA replication
5e-20 DNA metabolic process
3e-23 Ribonucleoprotein complex biogenesis
8e-27 Ribosome biogenesis
2e-19 RRNA processing
2e-20 RRNA metabolic process
2e-34 Regulation of localization
9e-35 Regulation of cellular component organization
1e-37 Protein localization
1e-40 Macromolecule localization
5e-37 Cellular localization
2e-34 Endocytosis
5e-42 Regulated exocytosis
2e-48 Exocytosis
6e-39 Secretion
4e-41 Secretion by cell
7e-34 Neutrophil mediated immunity
3e-34 Myeloid leukocyte mediated immunity
2e-106 Vesicle-mediated transport
7e-34 Catabolic process
8e-36 Small molecule metabolic process


A
hiPSCs-derived LSECs
Basal Medium
Component2 (31%)
Component1 (47%)
R²Y = 0.95; Q² = 0.78
B
-log10 (P)
log 2 (FC)
C
hiPSCs-derived LSECs
Basal Medium
leucine
valine
citramalic ac
succinic ac
glyceric ac
pyruvic ac
azelaic ac
mannitol
Phenylalanine
fructose
threonine
threitol
proline
lactic ac
mannose
ethanolamine
xylulose
lyxose
oxalic ac
glycolic ac
tagatose
picolonic ac
trans-4-hydroxy-L-
glucose
benzoic ac
sorbitol


A
1
2
3
4
5
6
7
-log10 (P)
0.5
1
1.5
2
2.5
3
3.5
0
0.1
0.2
0.3
0.4
0.5
Pathway impact
B
Galactose Metabolism
Glucose-Alanine Cycle
Fructose and Mannose Degradation
Warburg Effect
Gluconeogenesis
Transfer of Acetyl Groups into Mitochondria
Glycolysis
Glycine and Serine Metabolism
Valine, Leucine and Isoleucine Degradation
Citric Acid Cycle
Amino Sugar Metabolism
Lactose Degradation
Pyruvaldehyde Degradation
Phosphatidylethanolamine Biosynthesis
Ketone Body Metabolism
Phosphatidylcholine Biosynthesis
Pyruvate Metabolism
Glutamate Metabolism
Alanine Metabolism
Butyrate Metabolism
P value
1e-02
3e-01
7e-01
0
1
2
3
4
5
6
Fold Enrichment